^{19}F MRI of the Lungs Using Inert Fluorinated Gases: Challenges and New Developments

Marcus J. Couch, PhD,[1] Iain K. Ball, PhD,[2] Tao Li, MSc,[3] Matthew S. Fox, PhD,[4,5] Birubi Biman, MD; FRCPC,[6,7,8] and Mitchell S. Albert, PhD[3,7,9]*

Fluorine-19 (^{19}F) MRI using inhaled inert fluorinated gases is an emerging technique that can provide functional images of the lungs. Inert fluorinated gases are nontoxic, abundant, relatively inexpensive, and the technique can be performed on any MRI scanner with broadband multinuclear imaging capabilities. Pulmonary ^{19}F MRI has been performed in animals, healthy human volunteers, and in patients with lung disease. In this review, the technical requirements of ^{19}F MRI are discussed, along with various imaging approaches used to optimize the image quality. Lung imaging is typically performed in humans using a gas mixture containing 79% perfluoropropane (PFP) or sulphur hexafluoride (SF_6) and 21% oxygen. In lung diseases, such as asthma, chronic obstructive pulmonary disease (COPD), and cystic fibrosis (CF), ventilation defects are apparent in regions that the inhaled gas cannot access. ^{19}F lung images are typically acquired in a single breath-hold, or in a time-resolved, multiple breath fashion. The former provides measurements of the ventilation defect percent (VDP), while the latter provides measurements of gas replacement (ie, fractional ventilation). Finally, preliminary comparisons with other functional lung imaging techniques are discussed, such as Fourier decomposition MRI and hyperpolarized gas MRI. Overall, functional ^{19}F lung MRI is expected to complement existing proton-based structural imaging techniques, and the combination of structural and functional lung MRI will provide useful outcome measures in the future management of pulmonary diseases in the clinic.

Level of Evidence: 3
Technical Efficacy: Stage 1

J. MAGN. RESON. IMAGING 2019;49:343–354.

Magnetic resonance imaging (MRI) is a potentially ideal imaging modality for studying lung structure and function, as it is noninvasive, nonionizing, and it can be performed longitudinally. Although structural lung MRI has historically been poor, due to the low tissue density and other factors, ultrashort echo time (UTE)[1] and zero echo time (ZTE)[2] pulse sequences are now able to provide high-quality images of the lung parenchyma, airways, and blood vessels. These techniques have the potential to provide information that can assist with the management of respiratory disease. For example, in a study involving pediatric cystic fibrosis (CF) patients, UTE imaging was shown to detect structural abnormalities, such as airway wall thickening, bronchiectasis, and mucous plugging.[3] That study also showed that structural abnormality scores from UTE images were strongly correlated with scores obtained from computed tomography (CT) imaging. In addition to structural imaging, there has also been an interest in using proton-based imaging techniques to obtain functional information from the lungs. Imaging techniques such as oxygen-enhanced (OE) MRI[4] and Fourier decomposition (FD) MRI[5] can provide maps that are related to ventilatory function. Although OE and FD MRI techniques continue to improve,[6,7] both approaches suffer from a low signal-to-

View this article online at wileyonlinelibrary.com. DOI: 10.1002/jmri.26292

Received May 18, 2018, Accepted for publication Jul 26, 2018.

*Address reprint requests to: M.S.A., Thunder Bay Regional Health Research Institute, 980 Oliver Road, Thunder Bay, Ontario P7B 6V4, Canada. E-mail: albertmi@tbh.net

From the [1]Translational Medicine Program, The Hospital for Sick Children, Toronto, Ontario, Canada; [2]Philips Electronics Australia, North Ryde, Sydney, Australia; [3]Department of Chemistry, Lakehead University, Thunder Bay, Ontario, Canada; [4]Imaging Program, Lawson Health Research Institute, London, Ontario, Canada; [5]Department of Medical Biophysics, University of Western Ontario, London, Ontario, Canada; [6]Thunder Bay Regional Health Sciences Centre, Thunder Bay, Ontario, Canada; [7]Northern Ontario School of Medicine, Thunder Bay, Ontario, Canada; [8]Department of Medicine, McMaster University, Hamilton, Ontario, Canada; and [9]Thunder Bay Regional Health Research Institute, Thunder Bay, Ontario, Canada

noise ratio (SNR) and they are only indirectly sensitive to lung function.

Hyperpolarized (HP) helium-3 (^{3}He) and xenon-129 (^{129}Xe) MRI of the lungs has been performed for more than two decades,[8] and it continues to be a very active field of research in animals and humans. HP gas MRI is quickly evolving into a mature technique that is able to provide functional information regarding respiratory diseases, including chronic obstructive pulmonary disease (COPD), asthma, and CF.[9,10] HP gas MRI is a very versatile technique that is able to measure a range of functional biomarkers, such as the ventilation defect percent (VDP),[11] the apparent diffusion coefficient (ADC),[12] and fractional ventilation.[13] HP gas MRI is reproducible,[14] and imaging biomarkers are correlated with pulmonary function test (PFT) measurements, such as the forced expiratory volume in 1 second (FEV_1).[15] Unfortunately, the cost and complexity of HP gas MRI has played a role in hindering its widespread clinical use. HP gas MRI is currently only available in research centers, and it requires a polarizer, expensive isotopes, and dedicated trained personnel to manufacture the gases. Most research sites have switched to using HP ^{129}Xe only, since it is cheaper than ^{3}He and more widely available.[16] ^{129}Xe also has the advantage of being able to dissolve into blood and tissue, thereby providing information that is related to gas exchange.[16] Most HP ^{129}Xe studies in the literature have used isotopically enriched gas mixtures, which can also be expensive. Recent efforts have focused on optimizing polarizer technology and imaging approaches for cheaper, naturally abundant xenon gas mixtures[17]; however, the cost of purchasing a polarizer still represents a significant hurdle for new sites.

Fluorine-19 (^{19}F) MRI using inhaled inert fluorinated gases is a lung imaging technique currently under development that can potentially provide a more economical alternative to HP gas MRI. Feasibility studies have been reported in human lungs, demonstrating breath-hold images with gas mixtures containing 79% sulfur hexafluoride (SF_6) or perfluoropropane (C_3F_8 or PFP) and 21% oxygen (O_2).[18–20] SF_6 and PFP are nontoxic, abundant, and relatively inexpensive. Kruger et al reported cost estimates for ^{3}He, ^{129}Xe, and ^{19}F gases.[9] The per-liter cost of ^{3}He and enriched ^{129}Xe is much higher than ^{19}F gases, but the cost of naturally abundant xenon is similar to SF_6 and PFP. Since a typical imaging session using ^{19}F MRI might use several liters of SF_6 or PFP, the total cost of a single study might be approaching the cost of an enriched HP ^{129}Xe study; however, the advantage of ^{19}F lung imaging is that the gases are imaged using thermal equilibrium polarization and a polarizer system is not required.

Inert fluorinated gas MRI can potentially provide functional information that is similar to images obtained from HP gas MRI, such as images of the inhaled gas distribution and ventilation defects.[21] The purpose of this review is to provide an update on recent developments in ^{19}F MRI of inert fluorinated gases. The technical challenges of the technique are presented, along with a discussion of currently used imaging approaches. ^{19}F MRI is typically performed in either a single breath-hold, or during multiple breath-holds of the inhaled inert fluorinated gas mixture. Finally, preliminary comparisons to other pulmonary imaging techniques, such as FD and HP gas MRI, are discussed. ^{19}F lung MRI continues to be a developing technique, and future clinical studies will help to determine outcome measures that can be used to manage respiratory diseases and assist with the development of novel therapeutics.

Technical Challenges

Gas Properties

The physical properties of PFP and SF_6 have been previously discussed, along with a comparison with HP ^{3}He and ^{129}Xe, as well as OE MRI.[9,21] These properties will be briefly summarized in this section in order to discuss the technical requirements of ^{19}F MRI. ^{19}F has a high gyromagnetic ratio (~94% of the ^{1}H resonance) and a high natural abundance (100%). PFP and SF_6 are both heavy gases, with greater densities than ^{129}Xe and low self-diffusion coefficients. Perhaps the most notable difference from HP gases is the very short T_1 of PFP and SF_6 in the lungs (~1–20 msec compared to ~20 sec for ^{3}He and ^{129}Xe). For ^{3}He and ^{129}Xe, T_1 refers to a decay of the nonrenewable hyperpolarized signal, whereas inert fluorinated gases are not hyperpolarized and T_1 refers to a recovery of the longitudinal magnetization. SF_6 and PFP also have the advantage of having six magnetically equivalent ^{19}F nuclei per molecule. PFP has two additional ^{19}F nuclei that resonate ~48 ppm away from the primary spectral peak; however, they do not produce a discernable chemical shift artifact at typically used excitation bandwidths.

Since O_2 is paramagnetic, it strongly affects the T_1 of ^{129}Xe and ^{3}He through dipolar interactions. For this reason, HP gases are delivered in anoxic mixtures, and O_2 in the lungs reduces the T_1 from several hours (ie, ideal conditions with no O_2 present and a perfect magnetic environment),[22] to a few tens of seconds inside the lungs.[16] On the other hand, the T_1 relaxation of inert fluorinated gases is dominated by spin rotation interactions (ie, the coupling of nuclear spins to local magnetic fields produced by the rotation of large molecules),[23] and the T_1 is generally on the order of a few msec. Since the presence of O_2 has a much less dramatic effect on the T_1 of fluorinated gases than it does for HP gases, fluorinated gases can be mixed with O_2 to improve patient safety with little impact on image quality. Therefore, image acquisition can occur during continuous breathing of a gas mixture containing inert fluorinated gases and O_2. Overall, the combination of the above factors makes pulmonary ^{19}F MRI possible using thermally polarized inert fluorinated gases.

Hardware Requirements

Although inert fluorinated gas ^{19}F MRI does not require a polarizer system, there are a number of hardware requirements

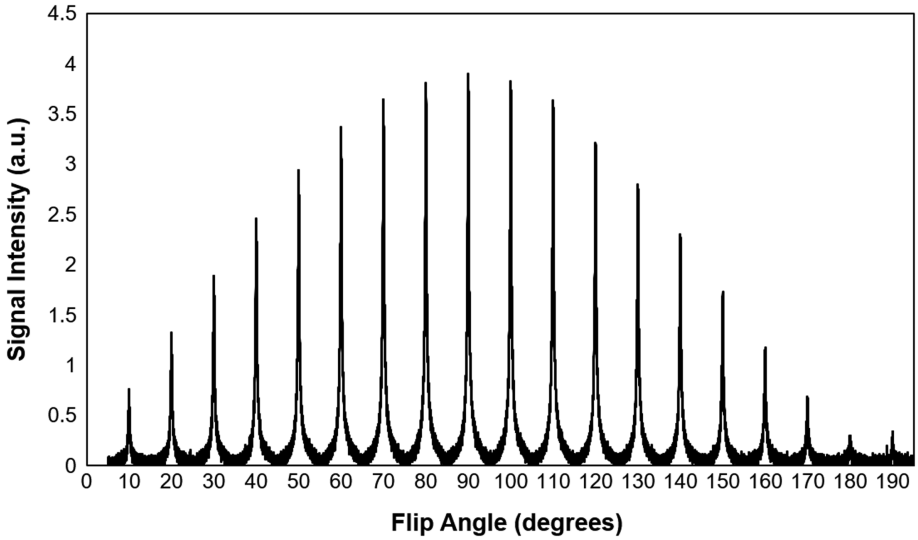

FIGURE 1: Flip angle calibration for ^{19}F MRI. ^{19}F free induction decays (FIDs) were acquired in increments of 10° in a bag filled with pure PFP. The transmitter gain was adjusted as needed, and the sequence was repeated until the 9th acquisition yields the highest possible signal intensity (ie, the 90° RF pulse).

that need to be met in order to perform lung imaging. Like HP ^{3}He and ^{129}Xe, a broadband multinuclear amplifier is required, despite the ^{19}F frequency being very close to the ^{1}H resonance. ^{19}F lung MRI has been performed at magnetic field strengths of 1.5T[24] and 3T,[19,20] but the optimal field strength remains unclear. Some recent work at 3T has noted that the ^{19}F acquisition could not be fully optimized due to specific absorption rate (SAR) limitations at the higher field strength.[25] ^{19}F MRI also requires custom-built radiofrequency (RF) coils tuned to the ^{19}F resonance frequency (40.05 MHz/T). An ideal RF coil should have full lung coverage and good B_1 homogeneity, but the coil should also be as small as patient comfort allows in order to minimize the RF power requirements and maximize receive sensitivity. Both single channel[19,20] and phased array ^{19}F RF coils[26] have been described for human lung imaging. Single channel flexible vest transmit/receive RF coils typically provide a good image quality, while maintaining patient comfort and compliance.[19,20] Other designs use a rigid elliptical birdcage transmit and a flexible receive array with up to 16 channels.[26] The rigid transmit coil should have a superior B_1 homogeneity, at the expense of requiring more RF power for the larger transmit element compared to the flexible vest. The use of a phased array receive coil allows for accelerated image acquisitions with parallel imaging reconstruction (ie, GRAPPA).[27]

There has also been an interest in developing dual-tuned ^{19}F/^{1}H coils, which provides the opportunity to acquire high-quality structural ^{1}H images without moving the subject. Dual-tuned ^{19}F/^{1}H coils are challenging to build, since the ^{19}F and ^{1}H frequencies are close to one another and coupling between the two channels will increase power requirements and reduce SNR. Dual-tuned ^{19}F/^{1}H coils have been demonstrated for animal imaging,[28–30] and human-sized coils are currently under development.[31] For human imaging, single-tuned ^{19}F coils need to be actively detuned in order to perform ^{1}H imaging with the body coil, which can be achieved using PIN diodes or microelectromechanical systems (MEMS) switches.[32] The ability to perform ^{1}H imaging while the subject is lying inside the ^{19}F coil allows for localization and planning of 3D ^{19}F acquisitions. It may also be possible to perform high-resolution structural ^{1}H imaging in this configuration; however, the image quality would likely benefit by changing the coil to a flexible phased array torso coil provided by the MRI manufacturer.

Software Requirements

Like HP gas MRI, the scanner is unable to perform automatic prescans with inert fluorinated gases and the calibration needs to be adjusted manually. In the case of HP gases, the flip angle can be calibrated by placing a syringe of HP gas inside the coil and acquiring free induction decays with a constant low flip angle. The measured flip angle can be extracted by fitting well-known signal equations to the acquired data,[33,34] and adjusting the transmitter gain as needed. In the case of inert fluorinated gases, the calibration can be performed using a flip angle sweep. Figure 1 shows a representative flip angle sweep consisting of 19 spectra acquired in 10° increments. In this case, the ^{19}F spectra were acquired in a 1L bag filled with pure PFP, and the transmitter gain was adjusted until the 90° RF pulse yielded the highest possible signal intensity. The coil calibration will likely change when loaded with a human subject, and therefore similar flip angle sweeps can be performed in a short breath-hold following inhalation of a 1L bag containing 79% PFP and 21% O_2.

In terms of data acquisition, SNR-efficient multinuclear pulse sequences are needed to overcome the low thermally polarized ^{19}F signal. Since inert fluorinated gases have a short T_1, short repetition times (TRs) can be used in combination

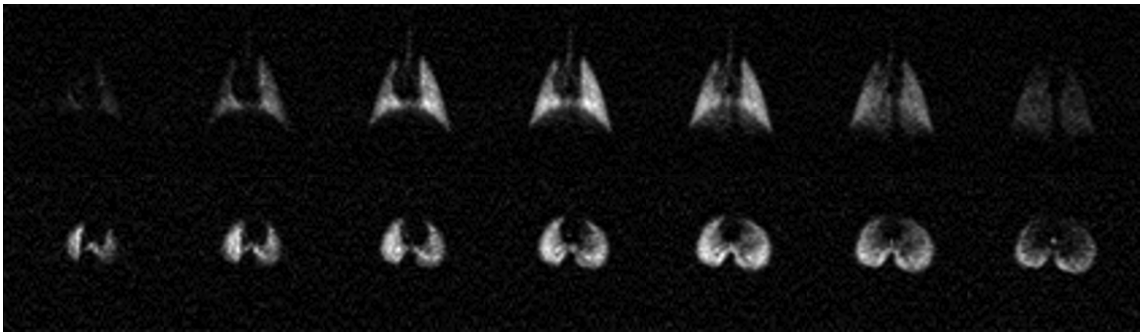

FIGURE 2: ^{19}F MR lung images obtained using a 3D gradient echo in a healthy rat. Coronal (top row) and axial (bottom row) images were obtained in separate acquisitions during free breathing of a mixture of 80% SF_6 and 20% O_2 (TR = 4 msec, TE = 0.85 msec, FOV = 75 × 75 mm^2, matrix = 64 × 64, 9 slices, thickness = 4 mm, FA = 70°, BW = 200 Hz/pix, 400 averages, scan duration = 5 min).

with a high flip angle. For example, the Ernst angle of 68° can be used when TR = T_1, and many signal averages can be acquired within a single breath-hold. The flip angle and TR are typically adjusted based on the pulse sequence requirements, the maximum output of the multinuclear RF amplifier, and SAR limitations. On the other hand, HP gases use a low flip angle and short TR, so that the reservoir of nonrecoverable magnetization can be steadily probed throughout the length of the image acquisition. Inert fluorinated gas MRI also requires a short echo time (TE), as PFP and SF_6 both have a short T_2^* in the lungs (1–2 msec at 3T).[19,35] The SNR can be further improved through the investigation of various *k*-space trajectories, such as gradient echoes,[20] UTE,[19] and steady-state free precession (SSFP) imaging.[36]

Gas Delivery

Similar to HP gas MRI, the gas delivery for ^{19}F MRI needs to be adequately controlled to ensure reproducible volumes and timing. Preclinical imaging typically involves anesthetized and mechanically ventilated animals, and an MR-compatible ventilator controls breathing rates, breath-holds, and gas mixtures for either air, O_2, HP gases,[37,38] or inert fluorinated gases.[35] In humans, HP gas imaging uses a dose volume that scales with subject size, such as 5 mL per kg of body weight,[39] or 1/6th of the total lung capacity.[40] The HP gas dose is typically balanced with nitrogen for a total 1L volume in a dose bag. The bag is inhaled from functional residual capacity (FRC), and breath-holds last up to 15 seconds. For ^{19}F MRI, larger dose volumes are used to image the lungs at a high concentration of the inert fluorinated gas. Therefore, several washin breaths of the inert fluorinated gas mixture may be needed in order to reach a steady-state concentration in the lungs.

Inert fluorinated gas delivery in human lung imaging can be accomplished using either large dose bags[19] or with a computer-controlled gas delivery system.[41] In the case of bag delivery, a large 5L dose bag of the inert fluorinated gas mixture is used to provide washin breaths (usually 79% PFP or SF_6 and 21% O_2). Subjects are coached to inhale calm breaths until the bag is empty. The 5L bag is then replaced with a full 1L bag of the PFP/O_2 mixture, and the subject is coached to inhale the 1L bag from FRC. Similar to HP gas MRI, lung imaging is then performed during a breath-hold at a total lung volume of FRC + 1L. ^{19}F lung MRI has also been performed in humans using a custom-built MR-compatible gas delivery system to deliver the PFP/O_2 mixture to subjects.[41] This system was able to switch the breathing mixture between air and PFP/O_2, and it provides real-time feedback such as O_2 saturation and the gas flow rate. Therefore, this system is ideal for ensuring patient safety, measuring gas tidal volumes, and gating image acquisitions.

Static Ventilation Imaging

Inert fluorinated gas MRI has been performed extensively in the lungs of animals since the 1980s, beginning with projection imaging in dogs and rabbits.[42,43] Since then, high-resolution 3D imaging has been demonstrated in rats,[44] and various animal studies have reported the measurement of functional biomarkers derived from inert fluorinated gas imaging, such as the ADC,[45,46] washin/washout kinetics,[47,48] fractional ventilation,[30,35] and the ventilation/perfusion ratio (V/Q).[49,50] Although PFP and SF_6 have been the most commonly used gases in recent years, some preclinical ^{19}F MRI studies have used hexafluoroethane (C_2F_6)[44] and tetrafluoromethane (CF_4).[43] Figure 2 shows representative ^{19}F lung MR images that were obtained in a healthy rat using a 3D gradient echo acquisition in the coronal (top row) and axial (bottom row) planes. These rat lung images were acquired during continuous ventilation with a mixture of 80% SF_6 and 20% O_2. No form of gating was used in these 5-minute acquisitions, and therefore the images represent an average point in the respiratory cycle between inspiration and expiration.

SF_6 was chosen for rat lung imaging in Fig. 2 due to its very short T_1 compared to PFP. SF_6 has a T_1 of ~1 msec,[21] and imaging can be performed under near Ernst angle conditions with a short TR (4 msec) and a flip angle of 70°. This combination of TR and flip angle is generally achievable due

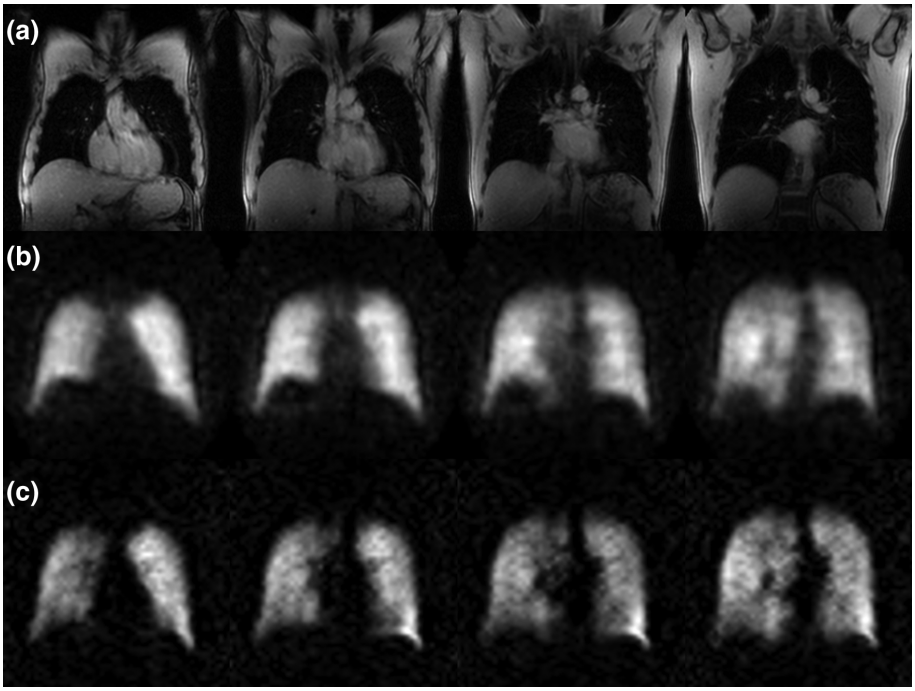

FIGURE 3: Comparison of (a) conventional ^{1}H, (b) ^{19}F 3D UTE, and (c) ^{19}F 3D gradient echo images acquired in the coronal plane from a healthy volunteer. ^{19}F UTE and gradient echo images were acquired in separate 15-second breath-holds, following several washin breaths of a mixture of 79% PFP and 21% O_2. ^{19}F 3D UTE imaging used the following settings: TR = 20 msec, TE = 0.2 msec, matrix = 64 × 64, FOV = 450 × 450 mm^2, 12 slices, 15 mm thickness, flip angle = 70°, 75% radial sampling density, 1 average, and BW = 140 Hz/pixel. ^{19}F 3D gradient echo images used the following settings: TR = 27 msec, TE = 1.12 msec, matrix = 64 × 64, 12 slices, in-plane FOV = 450 × 450 mm^2, 15 mm thickness, flip angle = 70°, partial echo factor = 62.5%, 2 averages, and BW = 200 Hz/pixel. The mean whole-lung SNR was 40 ± 17 and 18 ± 7, for UTE and gradient echo imaging, respectively. The UTE images were adapted, with permission, from Couch et al.[19]

to the low power requirements for small-animal RF coils. On the other hand, PFP has a T_1 of ~12–20 msec,[9,21] and a longer TR would be needed to achieve similar Ernst angle conditions with a high flip angle. Therefore, the shorter T_1 of SF_6 is advantageous for animal imaging, because more averaging is possible within a fixed scan duration (ie, a breath-hold).

The feasibility of human imaging using inert fluorinated gas MRI was first explored in explanted human lungs that were inflated with C_2F_6.[51] Although good-quality images were obtained, it was noted that ex vivo imaging benefits from a small RF coil design and an unlimited acquisition time. Naturally, in vivo imaging would involve larger RF coils that require more RF power, and image acquisitions would need to be limited to reasonable breath-hold durations. More recently, in vivo imaging has been performed in healthy volunteers,[18,19] in patients with COPD and asthma, and in patients who received lung transplants.[20] Although SF_6 and PFP have been used for human lung imaging, most studies have used PFP,[21] due to its ideal T_1 relaxation time. PFP has a T_1 of ~12 msec in human lungs at 3T,[19] and at a TR of 20 msec, the Ernst angle of 79° would yield the highest possible SNR efficiency. Lower flip angles have been used in the literature (ie, 40–70°), which is likely due to RF power and SAR limitations in larger human-sized coils.[19,20] Therefore, it is unlikely that SF_6 can be used optimally in human imaging.

Figure 3 shows a comparison of four central coronal slices from conventional ^{1}H, ^{19}F 3D UTE, and ^{19}F 3D gradient echo lung images that were acquired in a healthy volunteer in the same imaging session.[52] After several washin breaths of a mixture of 79% PFP and 21% O_2, the fluorinated gas mixture was expected to be at a steady-state concentration, and ^{19}F lung images were acquired during a 15-second breath-hold. Similar to HP gas MRI, both the UTE and gradient echo images had a ^{19}F signal that was fairly bright and homogeneous throughout the lungs of this healthy volunteer. Since PFP has a very fast transverse relaxation in the lungs (T_2^* ~2.2 msec at 3T), ^{19}F radial stack-of-stars UTE has been investigated in a feasible and SNR-efficient pulmonary imaging pulse sequence.[19] When compared with gradient echo imaging acquisitions that used a similar breath-hold duration, UTE images had a greater SNR. The short TE was expected to improve SNR in UTE imaging (TE = 0.2 msec compared to 1.12 msec for gradient echo), in addition to other factors such as oversampling at the center of *k*-space. The ^{19}F UTE images in Fig. 3 had a mean whole-lung SNR of 40 ± 17, while the 3D gradient echo images had an SNR of 18 ± 7. On the other hand, the gradient echo images show more detail (ie, better-defined edges in peripheral lung regions), while UTE images suffer from T_2^*-induced blurring (due to the relatively long acquisition window compared to T_2^*). Figure 4 shows a similar set of conventional ^{1}H, ^{19}F 3D UTE, and ^{19}F 3D gradient echo lung images that were acquired in another healthy volunteer in the axial plane,

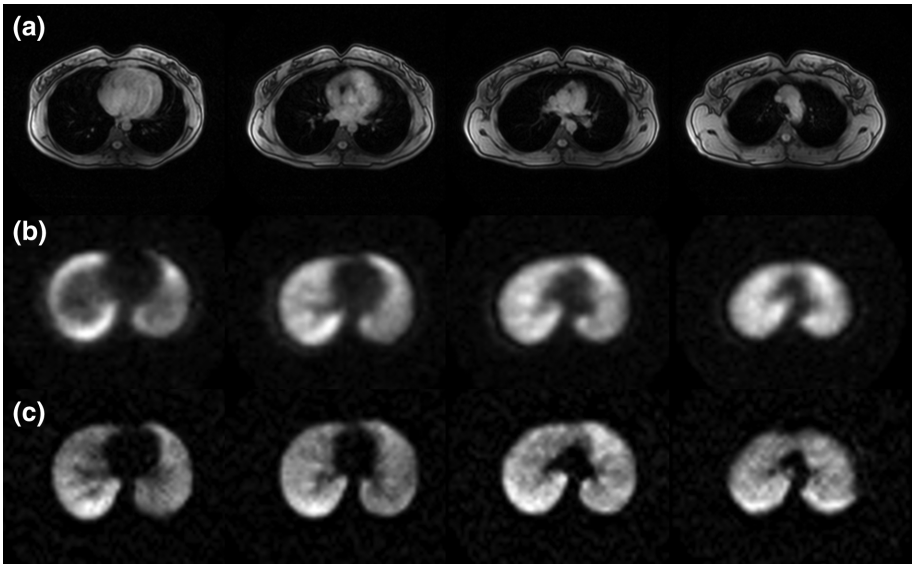

FIGURE 4: Comparison of (a) conventional ^{1}H, (b) ^{19}F 3D UTE, and (c) ^{19}F 3D gradient echo images acquired in the axial plane from a healthy volunteer. Image acquisition used the same methods as described in Fig. 3. The mean whole-lung SNR was 29 ± 13 and 21 ± 9, for UTE and gradient echo imaging, respectively. The UTE images were adapted, with permission, from Couch et al.[19]

and in this case a greater SNR is also apparent in the UTE images.

The majority of ^{19}F MRI human lung imaging reports to date have used gradient echo acquisitions, which sacrifices some SNR in favor of resolving fine details such as lung boundaries, airways, and vessels. A comparison of gradient echo imaging performed with single channel and phased-array RF coils has demonstrated an improved SNR in the phased-array RF coil, which is likely due to the use of smaller receive elements that have a high sensitivity.[27] In addition, the ability to accelerate image acquisitions will improve safety and tolerability for patients with severe lung diseases, such as COPD.[27] In recent years, several new sites have developed and implemented ^{19}F lung imaging technologies.[24,36,53,54] One report has described the feasibility of implementing ^{19}F MRI at a new site and performing lung imaging in healthy volunteers.[54] Others have focused on improving ^{19}F lung imaging by investigating novel RF coil designs,[32] and testing SNR-efficient pulse sequences, such as SSFP imaging.[36]

Similar to HP gas MRI, ventilation defects can be observed in ^{19}F MRI of patients with pulmonary diseases, where signal voids indicate the presence of airway obstructions and unventilated lung regions. Substantial ventilation heterogeneity has been reported in static breath-hold inert fluorinated gas images acquired in the lungs of patients with CF, COPD, and asthma.[20,53] These techniques may also provide functional information that can be used to assess the viability of transplanted lungs.[20] Like HP gas imaging, there has been an interest in quantifying ventilation heterogeneity with metrics such as the VDP. VDP is defined as the fraction of unventilated lung volume and it is calculated by coregistering the ventilation image with a conventional ^{1}H lung image. VDP measurements from HP gas MRI have used k-means segmentation,[39] as well as other linear binning approaches.[40,55] Preliminary ^{19}F MRI VDP measurements have used a signal intensity threshold for segmentation, and as expected, the VDP was strongly correlated with PFT measurements in COPD patients.[24]

Multiple Breath Imaging

The HP gas MRI literature has primarily performed static breath-hold imaging following a single breath washin of ^{3}He or ^{129}Xe, which provides a snapshot of lung function at a single timepoint.[16] With some adjustments to the gas delivery and image acquisition, time-resolved imaging can also be performed with multiple consecutive breath-holds during HP gas washin and/or washout.[37] Multiple breath HP gas imaging can be used to quantify gas replacement (ie, fractional ventilation), delayed filling, and gas trapping, which may be useful information in the assessment of obstructive lung diseases such as CF and COPD.[13,56] Acquiring and analyzing HP gas multiple breath imaging data requires careful corrections to account for the nonrenewable nature of the HP gas. On the other hand, inert fluorinated gas ^{19}F signal recovers quickly, and free-breathing can be performed with normoxic gas mixtures. A number of preclinical[47,48,57] and clinical[58,59] studies have used ^{19}F MRI to study inert gas washin/washout kinetics. One clinical study performed time-resolved imaging in patients with COPD, and the washin/washout curves were highly variable, reflecting ventilation heterogeneity.[59] Fractional ventilation mapping using multiple breath inert fluorinated gas MRI has recently been demonstrated in healthy rats,[35] in rat models of inflammation and fibrosis,[30] and in patients with COPD.[24,60]

Inert fluorinated gas fractional ventilation mapping was first demonstrated in rat lungs with a washout breathing

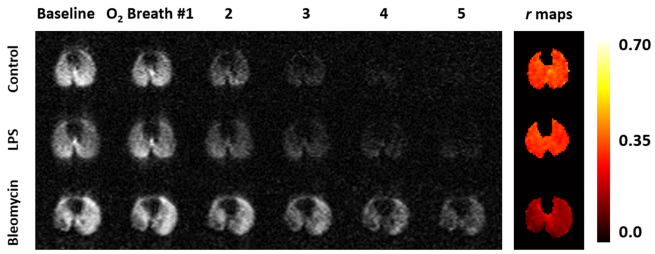

FIGURE 5: Fractional ventilation mapping using multiple breath inert fluorinated gas ^{19}F MRI in the lungs of rats. ^{19}F MRI captures the washout of SF_6, with three representative series of images obtained in a control rat, a rat instilled with lipopolysaccharide (to produce inflammation), and a rat instilled with bleomycin (to produce fibrosis). Each image in the washout series was a 2D whole-lung projection the axial plane (2D gradient echo, TR = 4 msec, TE = 0.48 msec, FOV = 75 × 75 mm^2, matrix = 64 × 64, slice thickness = 300 mm, FA = 70°, BW = 400 Hz/pixel, 65 averages, and partial echo factor = 0.505). The corresponding fractional ventilation maps are shown on the right, where a longer washout and reduced fractional ventilation results from the effects of inflammation and fibrosis. Modified, with permission, from Couch et al.[30]

scheme as follows[35]: at baseline the animal was ventilated with a mixture of 80% SF_6 and 20% O_2 for at least 3 minutes, and then a baseline ^{19}F image was acquired during a 10-second breath-hold. The breathing mixture was then switched to 100% O_2 for a total of nine breaths; a ^{19}F image was acquired during a 10-second breath-hold following each of the O_2 breaths. Each image in the washout series was acquired using a 2D x-centric pulse sequence, which provides the advantages of having both a short TE and a Cartesian *k*-space sampling approach.[61] Figure 5 shows three representative series of preclinical ^{19}F washout images obtained in a control rat, a rat instilled with lipopolysaccharide (LPS, to produce inflammation), and a rat instilled with bleomycin (to produce fibrosis).[30] The rat instilled with LPS has washout images that are similar to the control rat, while the rat instilled with bleomycin shows more ventilation heterogeneity and a slower SF_6 washout.

Fractional ventilation maps are calculated on a pixel-by-pixel basis by fitting the following signal equation to the acquired ^{19}F washout signal:

$$S(n) = C \cdot (1-r)^n, r = \frac{v_{fresh}}{v_{fresh} + v_{residual}}$$

where S is the signal at breath n, C is a proportionality constant, and r is the fractional ventilation, defined as the fractional refreshment of gas per breath (measured at end inspiration). HP gases would require additional factors in the proportionality constant to correct for T_1 and RF-induced signal decay, but the measured ^{19}F signal can essentially be treated as a density-weighted contrast and fitted without extensive corrections. Figure 5 also shows the fractional ventilation maps for the control rat, the LPS-instilled rat, and the bleomycin-instilled rat. The fractional ventilation was significantly reduced in the bleomycin-instilled rat, but the LPS-instilled washout was not significantly different from the control rat.[30]

Fractional ventilation mapping has also been reported in patients with COPD using multiple breath inert fluorinated gas ^{19}F imaging.[24] A combination of washin and washout imaging was performed using a previously described gas delivery device.[41] The washin phase consisted of imaging during breath-holds of 79% PFP and 21% O_2, while the washout phase consisted of continuous imaging during free-breathing with 100% O_2. Each image in the series was a 3D gradient echo, with a higher resolution image acquired during the washin phase (17-second breath-hold) and a lower-resolution image acquired during the free-breathing washout phase (2-second acquisition). The washout portion of the sequence took advantage of a phased-array RF coil to improve temporal resolution through undersampling. The inert fluorinated gas washin images were used to assess delayed filling by calculating VDP at two timepoints, representing initial and late phase washin.[24] Figure 6 shows examples of ^{19}F washin images obtained in two patients: one with GOLD stage I COPD and one with GOLD stage III COPD. Figure 6 also shows red masks overlaid on the ^{19}F washin images, representing ventilation defects determined by image segmentation. Similar to previous multiple breath HP gas imaging work, the initial phase VDP is high in COPD subjects, and after several breaths the gas is able to access more peripheral lung regions and the VDP decreases.[13] Figure 6 also shows maps of the washout time constant and fractional ventilation, which were calculated from the inert fluorinated gas washout images. As expected, the patient with GOLD stage III COPD had increased ventilation heterogeneity, and areas with long washout time constants correspond to areas with low fractional ventilation. Overall, ^{19}F fractional ventilation measurements were strongly correlated with PFTs,[24] and ventilation heterogeneity was qualitatively similar to previous HP gas studies that measured fractional ventilation in COPD[13] and CF.[56]

Comparison With Other Imaging Methods

Proton MRI

Since inert fluorinated gas ^{19}F MRI is a developing technique, most of the work to date has been performed in standalone studies using various image acquisition techniques and different parameters to optimize the image quality. As interest in this new pulmonary imaging technique is growing, validation studies and comparisons with existing pulmonary imaging techniques will be required in order to consider the multiple factors that contribute to image features and image quality, including the physical properties of these heavy fluorinated gases. One such study in COPD patients has compared ^{19}F MRI washout to fractional ventilation measurements

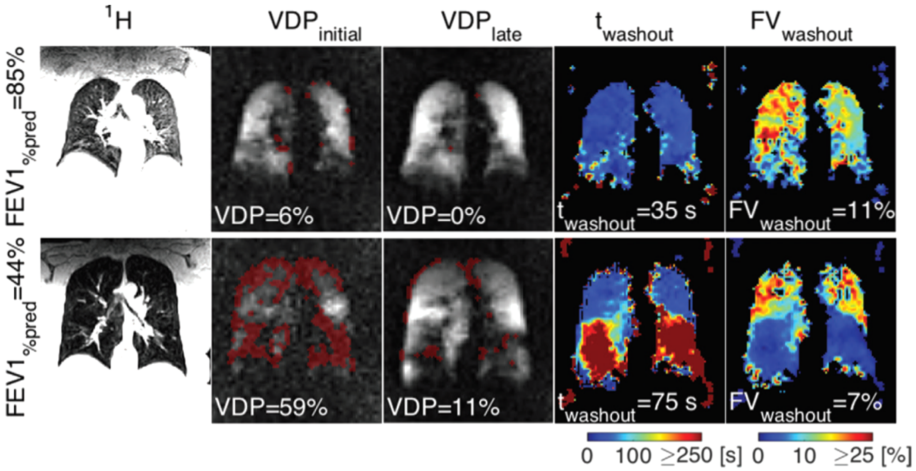

FIGURE 6: Multiple breath inert fluorinated gas ^{19}F MRI in COPD. The top row shows ^{19}F imaging results from a patient with GOLD stage I COPD, while the bottom row shows a patient with GOLD stage III COPD. From left to right, the panels show structural ^{1}H images, initial and late phase ^{19}F washin images (with a red mask indicating ventilation defects), a map of ^{19}F washout time constants, and a fractional ventilation map. Modified, with permission, from Gutberlet et al.[24]

obtained using FD MRI.[60] FD MRI is a ^{1}H-based technique that is able to obtain functional lung information without the use of a contrast agent.[5] This method rapidly acquires free-breathing lung images and uses a Fourier analysis of the lung signal in the temporal domain to decompose the periodic motion into ventilation and perfusion-weighted maps. FD MRI has been shown to be reproducible,[62] and it has also been validated with a comparison to HP ^{3}He MRI.[63] FD MRI has recently been extended to calculate fractional ventilation maps, and these results were correlated with PFTs and with ventilation defects observed in HP ^{3}He MRI.[64]

Figure 7 shows a comparison of FD-derived fractional ventilation and ^{19}F washout measurements obtained in three representative patients with COPD.[60] For all participants, the FD MRI and ^{19}F MRI measurements were strongly correlated. At GOLD stage I, the COPD patient had a homogeneous FD fractional ventilation and a fast ^{19}F washout. At GOLD stages II and III, the FD fractional ventilation decreases and the ^{19}F washout becomes longer. In addition, ventilation heterogeneity is increased in more severe COPD patients, suggesting the presence of gas trapping in slowly moving lung compartments. Overall, both imaging techniques appear to be sensitive to ventilation and lung function changes due to disease progression. In general, FD MRI is a technique that can be easily deployed on any MRI scanner, since it is a ^{1}H technique and no additional hardware or inhaled gases are required; however, FD MRI suffers from a low ^{1}H signal in the lungs. ^{19}F MRI has more specialized technical requirements, but the technique has the advantage

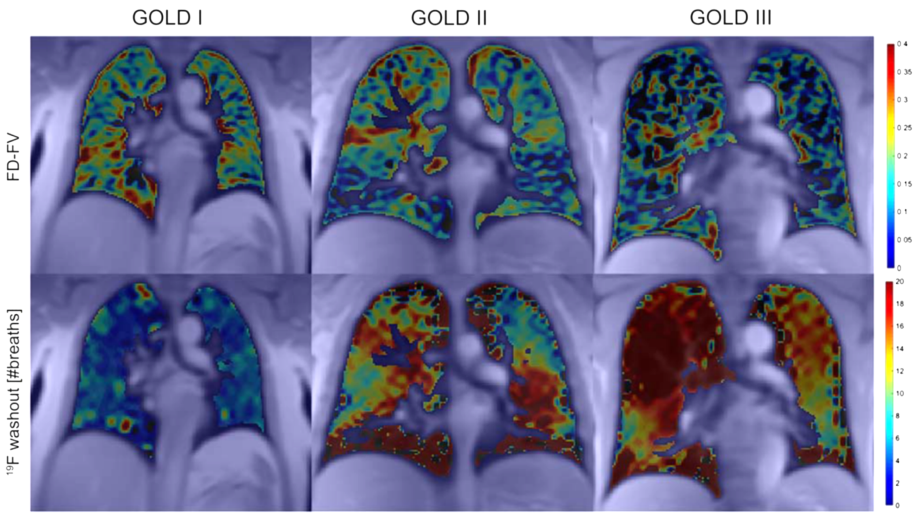

FIGURE 7: Comparison of Fourier decomposition (FD) MRI and inert fluorinated gas ^{19}F MRI. FD and ^{19}F MRI were performed in COPD patients with GOLD severity criteria ranging from stage I to stage III. FD measurements (top row) show fractional ventilation, while the ^{19}F measurements (bottom row) show the number of breaths required to washout the PFP gas (defined as the ^{19}F washout time constant multiplied by the breathing frequency). Image used with permission from Kaireit et al.[60]

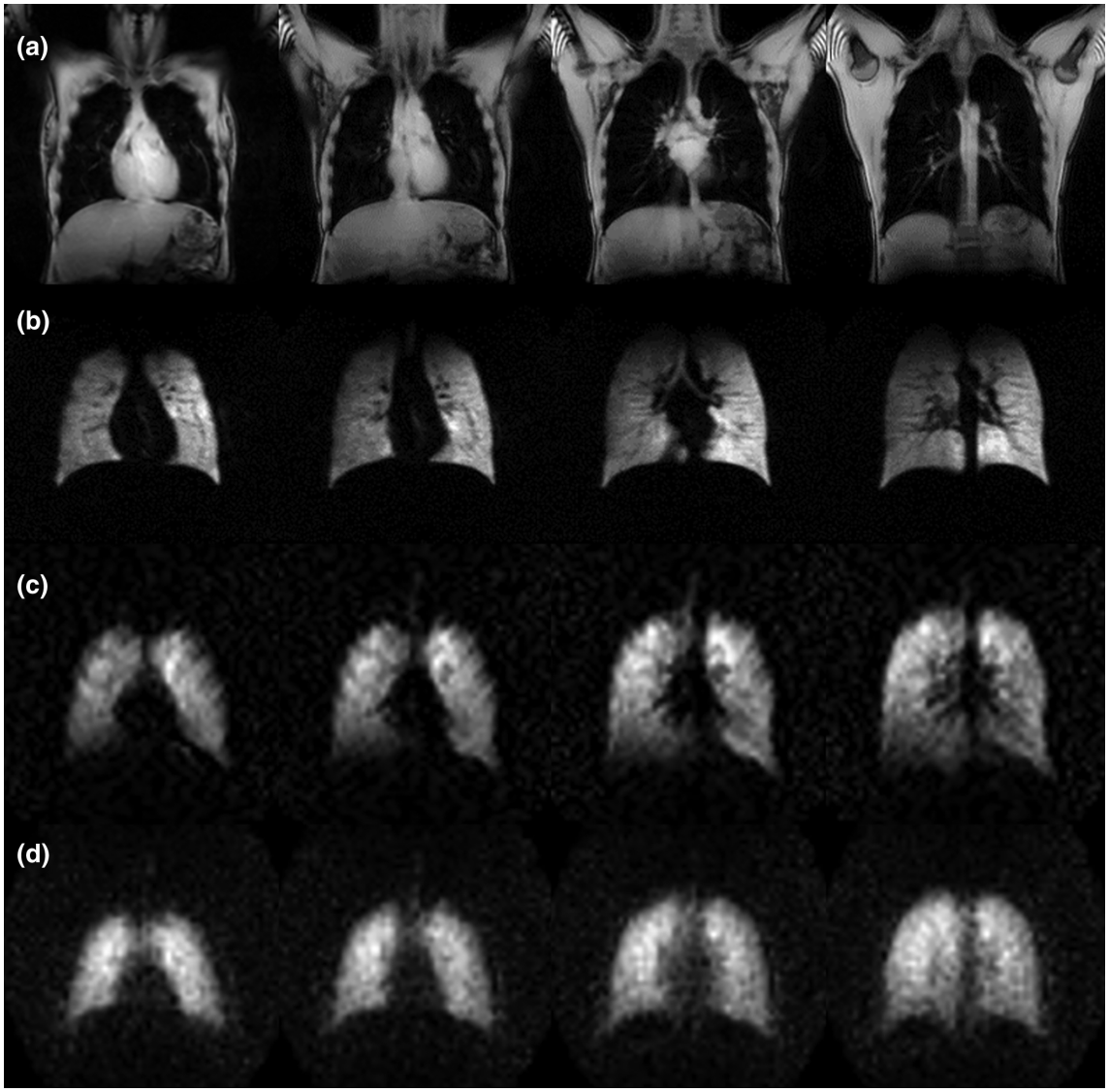

FIGURE 8: Comparison of (a) conventional ^{1}H, (b) HP ^{3}He 2D gradient echo, (c) ^{19}F 3D gradient echo, and (d) ^{19}F 3D UTE images acquired in the coronal plane from a healthy volunteer. The HP ^{3}He images were acquired during a 15-second breath-hold with a 330 mL dose of ^{3}He balanced to 1L with N_2. 2D multislice gradient echo ^{3}He images were acquired with the following settings: TR = 56 msec, TE = 1.53 msec, matrix = 128 × 64 reconstructed to 256 × 256, 14 slices, in-plane FOV = 450 × 450 mm^2, 15 mm thickness, flip angle = 7°, and BW = 500 Hz/pixel. The ^{19}F lung images were acquired using the same methods as described in Fig. 3.

of being able to directly image the inert fluorinated gases inside the lungs.

HP Gas MRI

HP ^{3}He and ^{129}Xe MRI are very well-established tools for mapping regional lung function in humans, and the applications of this technique have been discussed in a number of review articles.[9,16,65] Although inert fluorinated gas ^{19}F MRI is still a developing technique, ^{19}F images are expected to provide biomarkers that are similar to HP gas MRI.[21] Therefore, comparing images and biomarkers obtained from both techniques in a range of patient populations will be useful for validating ^{19}F MRI. There has been an interest in comparing VDP measurements between HP gas MRI and ^{19}F MRI,[66] but such a comparison has not yet been performed in subjects with pulmonary disease. Both techniques have significant technical requirements, such as a broadband multinuclear amplifier and custom-built RF coils; however, ^{19}F MRI is cheaper to implement, since a polarizer is not required.

Figure 8 shows a comparison of four central coronal slices that were obtained in a healthy volunteer using conventional ^{1}H, HP ^{3}He 2D gradient echo, ^{19}F 3D gradient echo, and ^{19}F 3D UTE imaging. Both ^{3}He and ^{19}F MRI were able to visualize a homogeneous distribution of inhaled gas inside the lungs. As expected, the SNR was significantly greater for HP ^{3}He MRI, while the ^{19}F images have a lower SNR and T_2^*-induced blurring is particularly apparent in the UTE images. Given the need for signal averaging in ^{19}F MRI and the limited breath-hold, a smaller matrix size was used at the same field of view (FOV). The HP ^{3}He images also show

more fine detail, such the major airways, which are afforded by the higher SNR and higher resolution compared to ^{19}F MRI. Other recent work has shown that ^{19}F and HP ^{129}Xe MRI compare favorably in healthy volunteers, although it was noted that the ^{19}F images were more homogeneous due to the lower acquired resolution.[67] It is possible that the current ^{19}F image quality could be useful for certain clinical applications; however, the technology will likely continue to be refined, as new pulse sequences and RF coil designs are being tested.

Outlook

Since there is a growing interest in lung imaging using ^{19}F MRI, it is worth noting that inert fluorinated gases are known to be potent greenhouse gases with long lifetimes.[68] Inert fluorinated gases have been used in numerous industrial applications, and atmospheric concentrations of these gases have been increasing in recent decades. Therefore, efforts will be made to capture and recycle the exhaled fluorinated gases. For example, an MR-compatible gas delivery system has been designed to use a non-rebreathing valve that isolates the inspiratory and expiratory gases, so that the exhaled gases can be collected in a large reservoir for purification and recycling.[41]

Technical developments in inert fluorinated gas MRI are ongoing, and there will be a strong focus on optimizing the image quality and improving SNR. At the same time, there is a desire to minimize breath-holds, especially for patients with severe lung disease. Various accelerated image acquisition techniques have been reported for HP gas MRI, including compressed sensing.[69] Inert fluorinated gas MRI usually requires long breath-hold acquisitions due to the need for signal averaging; however, the implementation of compressed sensing can provide good-quality images in manageable breath-holds as short as 6 seconds.[70,71] If the ^{19}F acquisition is short enough, it is possible that conventional ^{1}H images can also be acquired in the same breath-hold. Like HP gas imaging, having the ability to acquire perfectly coregistered ^{19}F and ^{1}H images would help to distinguish lung boundaries from unventilated signal defects.[72,73] On the other hand, high-resolution imaging may require an acquisition time that is longer than a breath-hold. In this case, a gated data acquisition could be performed during continuous breathing of the inert fluorinated gas, similar to HP gas imaging previously reported in animals.[74]

One interesting application of ^{19}F lung MRI is gas exchange mapping through the measurement of V/Q. Preclinical studies in rats have previously demonstrated V/Q mapping using a mixture of 30% SF_6 and 70% O_2.[49,50] This method takes advantage of the relationships between T_1, the partial pressure of the fluorinated gas, and the V/Q ratio. When the fluorinated gas mixture reaches a steady state concentration in the lungs, the ^{19}F signal accumulates in regions of the lung that have a low V/Q (ie, due to O_2 consumption). The increased fluorinated gas partial pressure leads to an increased T_1, which can be detected using either a Look–Locker or variable flip angle approach. T_1 and V/Q mapping have recently been performed in human lungs, and altered V/Q distributions were demonstrated in patients with COPD.[75,76] V/Q mapping can also be combined with inert fluorinated gas washout imaging to provide fractional ventilation maps in the same acquisition. This approach should provide valuable information in future studies of obstructive lung diseases.

Preliminary studies comparing ^{19}F MRI to HP gas and FD MRI appear to be promising, and these efforts will continue as novel pulse sequences are developed, and the techniques are tested in new patient populations. As researchers and clinicians consider the potential applications of inert fluorinated gas MRI, rigorous reproducibility and validation studies will be required. HP gas MRI technology is maturing, and instead of focusing on developing new acquisition approaches, investigators are now focusing on longitudinal imaging[77] and interventional trials with novel therapeutics.[78] ^{19}F MRI technology is not currently as well-developed as HP gases, but there is a strong potential for using it in similar applications in the future.

Conclusion

Overall, inert fluorinated gas MRI is a potentially feasible lung imaging technique that can be moved into the clinic. Inert fluorinated gas MRI does not require a polarizer, and it can be performed on any MRI scanner that is equipped with a ^{19}F RF coil and broadband multinuclear capabilities. Moreover, the reduced technical overhead associated with inert fluorinated gas MRI may provide a more straightforward path to clinical regulatory approvals, whereas HP gas MRI has met with obstacles. Although the SNR from ^{19}F lung MRI is currently lower than HP gas MRI, inert fluorinated gas MRI has the potential to yield meaningful functional information. Future clinical studies of inert fluorinated gas ^{19}F MRI will help to determine outcome measures that can be used to manage lung diseases longitudinally.

Acknowledgment

We thank the Thunder Bay Regional Health Sciences Centre (TBRHSC) MR technologists for their time and assistance with MR scanning of volunteers.

References

1. Johnson KM, Fain SB, Schiebler ML, Nagle S. Optimized 3D ultrashort echo time pulmonary MRI. Magn Reson Med 2013;70:1241–1250.
2. Gibiino F, Sacolick L, Menini A, Landini L, Wiesinger F. Free-breathing, zero-TE MR lung imaging. Magn Reson Mater Phys 2015;28:207–215.
3. Roach DJ, Cremillieux Y, Fleck RJ, et al. Ultrashort echo-time magnetic resonance imaging is a sensitive method for the evaluation of early cystic fibrosis lung disease. Ann Am Thorac Soc 2016;13:1923–1931.

4. Edelman RR, Hatabu H, Tadamura E, Li W, Prasad PV. Noninvasive assessment of regional ventilation in the human lung using oxygen-enhanced magnetic resonance imaging. Nat Med 1996;2: 1236–1239.
5. Bauman G, Puderbach M, Deimling M, et al. Non-contrast-enhanced perfusion and ventilation assessment of the human lung by means of Fourier decomposition in proton MRI. Magn Reson Med 2009;62:656–664.
6. Kruger SJ, Fain SB, Johnson KM, Cadman RV, Nagle SK. Oxygen-enhanced 3D radial ultrashort echo time magnetic resonance imaging in the healthy human lung. NMR Biomed 2014;27:1535–1541.
7. Capaldi DP, Sheikh K, Guo F, et al. Free-breathing pulmonary (1)H and hyperpolarized (3)He MRI: Comparison in COPD and bronchiectasis. Acad Radiol 2015;22:320–329.
8. Albert MS, Cates GD, Driehuys B, et al. Biological magnetic resonance imaging using laser-polarized 129Xe. Nature 1994;370:199–201.
9. Kruger SJ, Nagle SK, Couch MJ, Ohno Y, Albert M, Fain SB. Functional imaging of the lungs with gas agents. J Magn Reson Imaging 2016;43: 295–315.
10. Couch MJ, Blasiak B, Tomanek B, et al. Hyperpolarized and inert gas MRI: The future. Mol Imaging Biol 2015;17:149–162.
11. Kanhere N, Couch MJ, Kowalik K, et al. Correlation of lung clearance index with hyperpolarized 129Xe magnetic resonance imaging in pediatric subjects with cystic fibrosis. Am J Respir Crit Care Med 2017;196: 1073–1075.
12. Ouriadov A, Farag A, Kirby M, McCormack DG, Parraga G, Santyr GE. Lung morphometry using hyperpolarized (129) Xe apparent diffusion coefficient anisotropy in chronic obstructive pulmonary disease. Magn Reson Med 2013;70:1699–1706.
13. Hamedani H, Clapp JT, Kadlecek SJ, et al. Regional fractional ventilation by using multibreath wash-in (3)He MR imaging. Radiology 2016;279: 917–924.
14. Mathew L, Evans A, Ouriadov A, et al. Hyperpolarized 3He magnetic resonance imaging of chronic obstructive pulmonary disease: reproducibility at 3.0 Tesla. Acad Radiol 2008;15:1298–1311.
15. Fain SB, Panth SR, Evans MD, et al. Early emphysematous changes in asymptomatic smokers: detection with 3He MR imaging. Radiology 2006;239:875–883.
16. Mugler JP 3rd, Altes TA. Hyperpolarized 129Xe MRI of the human lung. J Magn Reson Imaging 2013;37:313–331.
17. Stewart NJ, Norquay G, Griffiths PD, Wild JM. Feasibility of human lung ventilation imaging using highly polarized naturally abundant xenon and optimized three-dimensional steady-state free precession. Magn Reson Med 2015;74:346–352.
18. Wolf U, Scholz A, Terekhov M, et al. Fluorine-19 MRI of the lung: first human experiment. In: Proc 16th Annual Meeting ISMRM, Toronto; 2008 (abstract 3207).
19. Couch MJ, Ball IK, Li T, et al. Pulmonary ultrashort echo time 19F MR imaging with inhaled fluorinated gas mixtures in healthy volunteers: feasibility. Radiology 2013;269:903–909.
20. Halaweish AF, Moon RE, Foster WM, et al. Perfluoropropane gas as a magnetic resonance lung imaging contrast agent in humans. Chest 2013; 144:1300–1310.
21. Couch MJ, Ball IK, Li T, et al. Inert fluorinated gas MRI: a new pulmonary imaging modality. NMR Biomed 2014;27:1525–1534.
22. Moller HE, Chen XJ, Saam B, et al. MRI of the lungs using hyperpolarized noble gases. Magn Reson Med 2002;47:1029–1051.
23. Chang YV, Conradi MS. Relaxation and diffusion of perfluorocarbon gas mixtures with oxygen for lung MRI. J Magn Reson 2006;181:191–198.
24. Gutberlet M, Kaireit TF, Voskrebenzev A, et al. Free-breathing dynamic (19)F gas MR imaging for mapping of regional lung ventilation in patients with COPD. Radiology 2018;286:1040–1051.
25. Maunder A, Rao M, Wild J. Optimization of steady-state free precession with 19f perfluoropropane for increased signal-to-noise for human lung ventilation imaging at 3 T. In: Proc 26th Annual Meeting ISMRM, Paris; 2018 (abstract 2470).
26. Gutberlet M, Voskrebenzev A, Kern A, et al. Repeatability of regional lung ventilation quantification using 19F fluorinated gas washout magnetic resonance imaging in free breathing. In: Proc 25th Annual Meeting ISMRM, Honolulu; 2017 (abstract 3311).
27. Charles HC, Jones RW, Halaweish AF, Ainslie MD. Parallel imaging for short breath hold times in perfluorinated gas imaging of the lung. In: Proc 23rd Annual Meeting ISMRM, Toronto; 2015 (abstract 3984).
28. Hu L, Hockett FD, Chen J, et al. A generalized strategy for designing (19) F/(1)H dual-frequency MRI coil for small animal imaging at 4.7 Tesla. J Magn Reson Imaging 2011;34:245–252.
29. Gajawada G, Li T, Couch MJ, Fox MS, Albert MS. A 19F - 1H linear dual tuned RF birdcage coil for rat lung imaging at 3T. In: Proc 23rd Annual Meeting ISMRM, Toronto; 2015 (abstract 1461).
30. Couch MJ, Fox MS, Viel C, et al. Fractional ventilation mapping using inert fluorinated gas MRI in rat models of inflammation and fibrosis. NMR Biomed 2016;29:545–552.
31. Kampani VV, Jones RW, Charles HC, Hussey N. Dual-Tuned RF Coil system for Parallel Imaging of Human Lungs Using Perfluorinated Gases. In: Proc 25th Annual Meeting ISMRM, Honolulu; 2017 (abstract 2665).
32. Maunder A, Rao M, Robb FJL, Wild JM. Combined transmit array and 8-channel receive coil array for 19F/1H for human lung imaging at 1.5 T utilizing MEMS transmit-receive detuning. In: Proc 25th Annual Meeting ISMRM, Honolulu; 2017 (abstract 1052).
33. Zhao L, Mulkern R, Tseng CH, et al. Gradient-echo imaging considerations for hyperpolarized Xe-129 MR. J Magn Reson Ser B 1996;113: 179–183.
34. Miller GW, Altes TA, Brookeman JR, De Lange EE, Mugler JP 3rd. Hyperpolarized 3He lung ventilation imaging with B1-inhomogeneity correction in a single breath-hold scan. Magn Reson Mater Phys 2004;16: 218–226.
35. Ouriadov AV, Fox MS, Couch MJ, Li T, Ball IK, Albert MS. In vivo regional ventilation mapping using fluorinated gas MRI with an x-centric FGRE method. Magn Reson Med 2015;74:550–557.
36. Maunder A, Stewart NJ, Rao M, Robb FJL, Wild JM. Steady-state free precession for improved signal to noise in lung ventilation imaging with 19F perfluoropropane at 1.5 T. In: Proc 25th Annual Meeting ISMRM, Honolulu; 2017 (abstract 3318).
37. Couch MJ, Ouriadov A, Santyr GE. Regional ventilation mapping of the rat lung using hyperpolarized 129Xe magnetic resonance imaging. Magn Reson Med 2012;68:1623–1631.
38. Nouls J, Fanarjian M, Hedlund L, Driehuys B. A constant-volume ventilator and gas recapture system for hyperpolarized gas MRI of mouse and rat lungs. Concepts Magn Reson Part B Magn Reson Eng 2011;39B: 78–88.
39. Kirby M, Heydarian M, Svenningsen S, et al. Hyperpolarized 3He magnetic resonance functional imaging semiautomated segmentation. Acad Radiol 2012;19:141–152.
40. Thomen RP, Walkup LL, Roach DJ, Cleveland ZI, Clancy JP, Woods JC. Hyperpolarized 129Xe for investigation of mild cystic fibrosis lung disease in pediatric patients. J Cyst Fibros 2017;16:275–282.
41. Halaweish AF, Charles HC. Physiorack: An integrated MRI safe/conditional, Gas delivery, respiratory gating, and subject monitoring solution for structural and functional assessments of pulmonary function. J Magn Reson Imaging 2014;39:735–741.
42. Heidelberger E, Lauterbur PC. Gas phase 19F-NMR zeugmatography: a new approach to lung ventilation imaging. In: Proc 1st Annual Meeting Society of Magnetic Resonance in Medicine, 1982 (abstract p 70–71).
43. Rinck PA, Petersen SB, Lauterbur PC. NMR-Imaging von fluorhaltigen Substanzen. 19Fluor-Ventilations- und -Perfusionsdarstellungen. Fortschr Röntgenstr 1984;140:239–243.
44. Kuethe DO, Caprihan A, Fukushima E, Waggoner RA. Imaging lungs using inert fluorinated gases. Magn Reson Med 1998;39:85–88.

45. Perez-Sanchez JM, Perez de Alejo R, Rodriguez I, Cortijo M, Peces-Barba G, Ruiz-Cabello J. In vivo diffusion weighted 19F MRI using SF6. Magn Reson Med 2005;54:460–463.

46. Carrero-Gonzalez L, Kaulisch T, Stiller D. In vivo diffusion-weighted MRI using perfluorinated gases: ADC comparison between healthy and elastase-treated rat lungs. Magn Reson Med 2013;70:1761–1764.

47. Schreiber WG, Eberle B, Laukemper-Ostendorf S, et al. Dynamic 19F-MRI of pulmonary ventilation using sulfur hexafluoride (SF6) gas. Magn Reson Med 2001;45:605–613.

48. Scholz AW, Wolf U, Fabel M, et al. Comparison of magnetic resonance imaging of inhaled SF6 with respiratory gas analysis. Magn Reson Imaging 2009;27:549–556.

49. Kuethe DO, Caprihan A, Gach HM, Lowe IJ, Fukushima E. Imaging obstructed ventilation with NMR using inert fluorinated gases. J Appl Physiol 2000;88:2279–2286.

50. Adolphi NL, Kuethe DO. Quantitative mapping of ventilation-perfusion ratios in lungs by 19F MR imaging of T1 of inert fluorinated gases. Magn Reson Med 2008;59:739–746.

51. Jacob RE, Chang YV, Choong CK, et al. 19F MR imaging of ventilation and diffusion in excised lungs. Magn Reson Med 2005;54:577–585.

52. Couch MJ, Ball IK, Li T, et al. Optimized strategies for 19F MRI of human lungs and comparison of UTE and gradient echo imaging. In: Proc 22nd Annual Meeting ISMRM, Milan; 2014 (abstract 777).

53. Lee Y, Akinnagbe-Zusterzeel E, Goralski J, et al. 19F ventilation imaging of cystic fibrosis patients. In: Proc 24th Annual Meeting ISMRM, Singapore; 2016 (abstract 1607).

54. Pippard B, Neal M, Dutta P, Simpson AJ, Thelwall P. 19F-MRI of inhaled perfluoropropane gas: a novel approach to ventilation imaging. Thorax 2017;72:A157–A158.

55. He M, Kaushik SS, Robertson SH, et al. Extending semiautomatic ventilation defect analysis for hyperpolarized (129)Xe ventilation MRI. Acad Radiol 2014;21:1530–1541.

56. Horn FC, Deppe MH, Marshall H, Parra-Robles J, Wild JM. Quantification of regional fractional ventilation in human subjects by measurement of hyperpolarized 3He washout with 2D and 3D MRI. J Appl Physiol 2014; 116:129–139.

57. Wolf U, Scholz A, Terekhov M, Koebrich R, David M, Schreiber LM. Visualization of inert gas wash-out during high-frequency oscillatory ventilation using fluorine-19 MRI. Magn Reson Med 2010;64:1478–1483.

58. Charles C, Soher B, Halaweish AF. Modeling of the spatio-temporal distribution of pulmonary ventilation via perfluoropropane gas enhanced MRI. In: Proc American Thoracic Society; 2015 (abstract A2125).

59. Halaweish AF, Foster WM, Moon RE, MacIntyre NR, MacFall JR, Charles HC. Dynamics of pulmonary ventilation distribution at steady state via 19fluorine-enhanced MRI: Initial experiences and future developments. In: Proc 21st Annual Meeting ISMRM, Salt Lake City; 2013 2013 (abstract 4111).

60. Kaireit TF, Gutberlet M, Voskrebenzev A, et al. Comparison of quantitative regional ventilation-weighted fourier decomposition MRI with dynamic fluorinated gas washout MRI and lung function testing in COPD patients. J Magn Reson Imaging 2018;47:1534–1547.

61. Ouriadov AV, Santyr GE. High spatial resolution hyperpolarized 3 He MRI of the rodent lung using a single breath X-centric gradient-recalled echo approach. Magn Reson Med 2017;78:2334–2341.

62. Lederlin M, Bauman G, Eichinger M, et al. Functional MRI using Fourier decomposition of lung signal: reproducibility of ventilation- and perfusion-weighted imaging in healthy volunteers. Eur J Radiol 2013;82: 1015–1022.

63. Bauman G, Scholz A, Rivoire J, et al. Lung ventilation- and perfusion-weighted Fourier decomposition magnetic resonance imaging: in vivo validation with hyperpolarized 3He and dynamic contrast-enhanced MRI. Magn Reson Med 2013;69:229–237.

64. Capaldi DPI, Eddy RL, Svenningsen S, et al. Free-breathing pulmonary MR imaging to quantify regional ventilation. Radiology 2018;287: 693–704.

65. Santyr G, Kanhere K, Morgado F, Rayment JH, Ratjen F, Couch MJ. Hyperpolarized gas magnetic resonance imaging of pediatric cystic fibrosis lung disease. Acad Radiol 2018 [Epub ahead of print].

66. Couch MJ, Ball IK, Li T, Fox MS, Biman B, Albert MS. Comparing pulmonary MRI using inert fluorinated gases and hyperpolarized 3He: Is 19F MRI good enough? In: Proc 23rd Annual Meeting ISMRM, Toronto; 2015 2015 (abstract 1501).

67. Maunder A, Hughes P, Chan H, et al. Comparing 19F C3F8 lung ventilation imaging with hyperpolarized 129Xe: Similarities and limitations. In: Proc 26th Annual Meeting ISMRM, Paris; 2018 (abstract 1085).

68. Khalil MAK, Rasmussen RA, Culbertson JA, Prins JM, Grimsrud EP, Shearer MJ. Atmospheric perfluorocarbons. Environ Sci Technol 2003; 37:4358–4361.

69. Ajraoui S, Parra-Robles J, Marshall H, Deppe MH, Clemence M, Wild JM. Acquisition of (3)He ventilation images, ADC, T(2)* and B(1) maps in a single scan with compressed sensing. NMR Biomed 2012;25:44–51.

70. Maunder A, Collier G, Robb F, Rao M, Wild J. Evaluation of sparse sampling for improved image quality of 19F fluorinated gas lung ventilation MRI. In: Proc 26th Annual Meeting ISMRM, Paris; 2018 (abstract 3538).

71. Neal M, Pippard B, Hollingsworth K, Thelwall P. Accelerated 19F-MR imaging of inhaled perfluoropropane for assessment of pulmonary ventilation. In: Proc 26th Annual Meeting ISMRM, Paris; 2018 (abstract 2474).

72. Wild JM, Ajraoui S, Deppe MH, et al. Synchronous acquisition of hyperpolarised 3He and 1H MR images of the lungs — maximising mutual anatomical and functional information. NMR Biomed 2011;24:130–134.

73. Rao M, Wild JM. RF instrumentation for same-breath triple nuclear lung MR imaging of (1)H and hyperpolarized (3)He and (129)Xe at 1.5T. Magn Reson Med 2016;75:1841–1848.

74. Driehuys B, Walker J, Pollaro J, et al. 3He MRI in mouse models of asthma. Magn Reson Med 2007;58:893–900.

75. Obert A, Gutberlet M, Rotärmel A, Wacker F, Vogel-Claussen J. Mapping of ventilation/perfusion ratios in the human lung using 19F MRI of perfluoropropane. In: Proc 26th Annual Meeting ISMRM, Paris; 2018 (abstract 2473).

76. Gutberlet M, Obert A, Voskrebenzev A, Klimes F, Wacker F, Vogel-Claussen J. Quantification of gas concentration and fractional ventilation using high temporal resolution MRI of pulmonary fluorinated (19F) gas washin dynamics in free breathing. In: Proc 26th Annual Meeting ISMRM, Paris; 2018 (abstract 1084).

77. Smith L, Marshall H, Aldag I, et al. Longitudinal assessment of children with mild cystic fibrosis using hyperpolarized gas lung magnetic resonance imaging and lung clearance index. Am J Respir Crit Care Med 2018;197:397–400.

78. Altes TA, Johnson M, Fidler M, et al. Use of hyperpolarized helium-3 MRI to assess response to ivacaftor treatment in patients with cystic fibrosis. J Cyst Fibros 2017;16:267–274.